INTERFACE

rsif.royalsocietypublishing.org

Research

Cite this article: Agrawal DK, Franco E, Schulman R. 2015 A self-regulating biomolecular comparator for processing oscillatory signals. *J. R. Soc. Interface* **12**: 20150586.
http://dx.doi.org/10.1098/rsif.2015.0586

Received: 1 July 2015
Accepted: 26 August 2015

Subject Areas:
bioengineering, synthetic biology, systems biology

Keywords:
biomolecular comparator, oscillator, modular, synthetic biology, dynamical systems

Author for correspondence:
Rebecca Schulman
e-mail: rschulm3@jhu.edu

Electronic supplementary material is available at http://dx.doi.org/10.1098/rsif.2015.0586 or via http://rsif.royalsocietypublishing.org.

THE ROYAL SOCIETY PUBLISHING

A self-regulating biomolecular comparator for processing oscillatory signals

Deepak K. Agrawal[1], Elisa Franco[3] and Rebecca Schulman[1,2]

[1]Department of Chemical and Biomolecular Engineering, and [2]Department of Computer Science, Johns Hopkins University, Baltimore, MD 21218, USA
[3]Department of Mechanical Engineering, University of California at Riverside, 900 University Avenue, Riverside, CA 92521, USA

While many cellular processes are driven by biomolecular oscillators, precise control of a downstream on/off process by a biochemical oscillator signal can be difficult: over an oscillator's period, its output signal varies continuously between its amplitude limits and spends a significant fraction of the time at intermediate values between these limits. Further, the oscillator's output is often noisy, with particularly large variations in the amplitude. In electronic systems, an oscillating signal is generally processed by a downstream device such as a comparator that converts a potentially noisy oscillatory input into a square wave output that is predominantly in one of two well-defined on and off states. The comparator's output then controls downstream processes. We describe a method for constructing a synthetic biochemical device that likewise produces a square-wave-type biomolecular output for a variety of oscillatory inputs. The method relies on a separation of time scales between the slow rate of production of an oscillatory signal molecule and the fast rates of intermolecular binding and conformational changes. We show how to control the characteristics of the output by varying the concentrations of the species and the reaction rates. We then use this control to show how our approach could be applied to process different *in vitro* and *in vivo* biomolecular oscillators, including the p53-Mdm2 transcriptional oscillator and two types of *in vitro* transcriptional oscillators. These results demonstrate how modular biomolecular circuits could, in principle, be combined to build complex dynamical systems. The simplicity of our approach also suggests that natural molecular circuits may process some biomolecular oscillator outputs before they are applied downstream.

1. Introduction

Biomolecular circuits with well-defined dynamics are central to the control of temporal behaviours in biology. One prototypical such circuit is the biomolecular oscillator, which plays essential roles in the control of the cell cycle, circadian rhythms and other rhythmic processes such as muscle contraction [1–3]. In each of these oscillatory processes, coupled chemical reactions collectively produce one or more species whose concentrations vary periodically between high and low values. While a variety of naturally occurring or artificial biomolecular oscillators have been described [2–7], each of these systems has important performance limitations. Oscillations generally occur only within a fairly narrow range of parameter values, and a given architecture may not allow particular amplitudes or periods. The shape of the oscillatory signal also cannot generally be changed. One particular challenge that arises because of the shape of the oscillatory output is that a biomolecular oscillator's output spends most of its time at concentrations between the maximum and minimum, making it difficult to control downstream processes that switch between on and off states. The limited ability to tune a biomolecular oscillator signal means either that the downstream process controlled by the oscillator must adapt to the dynamics of the oscillator or that the oscillator signal must be processed further by, for example, signalling molecules or transcriptional control, with the processed output being used to control a process of interest.

Electronic circuits also use oscillatory signals for applications such as frequency generation and signal clocking, and face similar design challenges, in that the oscillatory signal's shape and amplitude cannot be tuned arbitrarily. To address this problem, electronic circuits use a variety of 'post-processing' circuits to produce an output signal that stably controls a downstream process of interest. For example, an electronic clock often incorporates an amplitude-limiting mechanism such as a comparator that modulates the oscillatory analogue response into a square-wave digital signal. The comparator also minimizes intrinsically or extrinsically generated amplitude variations [8] and robustly switches between fully on and fully off states during different periods of a cycle without spending a significant fraction of the time in an intermediate state. This alternating on/off signal can in turn switch downstream devices on and off.

In this paper, we describe an amplitude-limiting chemical reaction network that could be used to translate the output signal of a time-varying biomolecular species into a reliable on and off signal. We describe a generic set of chemical reactions and rate constants that could conceivably be implemented either *in vitro* or *in vivo* using a set of biomolecular reactions that were proposed earlier as a mechanism for sharpening a spatial chemical gradient [9]. We then consider what rate constants and reactant concentrations are needed for the comparator to function effectively with existing biomolecular oscillators. In order to ensure that the system could potentially be assembled both *in vitro* and *in vivo*, we use reaction rates that are feasible for components of DNA strand displacement networks [10,11], for *in vitro* transcriptional networks and for *in vivo* regulatory networks [12–14]. Importantly, we show how the comparator we describe can process a wide variety of oscillatory inputs [4–7] given appropriate rate constants for the component reactions. The reactions we describe work well because there is a time-scale separation between the production of the oscillatory source species and the reactions that produce an amplitude-controlled output. Similar principles of time-scale separation have been observed or applied in different biological, electrical and mechanical systems [15–17].

2. Material and methods

2.1. Comparator design

Our goal was to develop a set of coupled chemical reactions that can convert an oscillatory species into a dynamic molecular signal that rapidly switches between low and high concentration limits by acting as a biomolecular comparator. The output of these chemical reactions should be independent of variation in the amplitude between periods. Such reactions would robustly propagate the period of the oscillatory signal and produce a predefined amplitude response while suppressing variation in the amplitude limits and random fluctuations in concentration. Further, our goal was for these reactions to operate modularly, in order to ensure that the upstream reactions, which are producing the oscillatory input to the comparator, remain unaffected by the new downstream reactions. This modularity is important, because the load placed on an oscillator when additional signal is added or removed can significantly alter the oscillator's performance [6,17].

Recently, Scalise & Schulman [9] proposed a set of reactions, or module, to control the spatial response of a reaction–diffusion system. Here, we show that these reactions can also be used to control the temporal response of an oscillating input species. The reactions work by comparing the input species with a thresholding species and then using the result of this comparison to dictate the output, i.e. they rely on ultrasensitivity by molecular titration [18]. A high concentration of output should be produced when the source species is above the threshold; otherwise, a low concentration of output should be produced. To make it possible to control the concentration and range of the output species, the signal produced by the thresholding signal is amplified, and saturates at a defined concentration. The set of chemical reactions that describe the operation of the biomolecular comparator are as follows:

$$S \xrightarrow{k_p^I} I + S, \tag{2.1}$$

$$I \xrightarrow{k_d^I} \emptyset, \tag{2.2}$$

$$I + T \xrightarrow{k_r^T} \emptyset, \tag{2.3}$$

$$I + A \xrightarrow{k_r^A} I + O, \tag{2.4}$$

$$P_T \xrightarrow{k_p^T} P_T + T, \tag{2.5}$$

$$T \xrightarrow{k_d^T} \emptyset, \tag{2.6}$$

$$P_A \xrightarrow{k_p^A} P_A + A, \tag{2.7}$$

$$A \xrightarrow{k_d^A} \emptyset \tag{2.8}$$

and

$$O \xrightarrow{k_d^O} \emptyset, \tag{2.9}$$

where S is the source signal from the oscillator and O is the output of the module. I, T and A are intermediates, which we refer to as the input, thresholding and amplifying species, respectively. The function of reaction (2.1) is to produce an input species, I, whose level depends on the current output of the oscillator, S, without placing a load on S. In this reaction, S catalyses the conversion of an abundant input into I. Effectively, in reactions (2.1) and (2.2), S is reproduced as I via a proportional controller mechanism. Reactions (2.3) and (2.4) process signal I to produce an output species. Specifically, in reaction (2.3), as I is produced, an intermediate species T degrades a set amount of I into waste. The concentration of T serves as a low threshold for I; when $[I]$ is smaller than $[T]$, the output produced by the comparator is set at the low level. In reaction (2.4), the remaining amount of I catalyses the conversion of another intermediate species A into the output O. This output is set as the high level. To ensure a dynamic response, I, T and A are constantly produced and degraded (reactions (2.1), (2.2), (2.5)–(2.8)). *In vivo*, this mechanism implies that T and A would be produced (or activated) constitutively, whereas S catalyses the production of I; I further accelerates the degradation of T, and converts A into O.

In reaction (2.1), we assume that the substrate transformed by S into I remains at a constant concentration, so it is not explicitly modelled. The same condition holds for P_T and P_A, which are used to produce T and A respectively, so these species are also modelled as having constant concentrations. *In vivo*, the stability of precursor concentrations could be achieved through buffering [19], whereas *in vitro*, high concentrations of these precursors could cause them to remain effectively constant over long time periods [9,20].

2.2. Differential equations

Using the law of mass action, the kinetics of the biomolecular comparator can be modelled as

$$\frac{\mathrm{d}[I]}{\mathrm{d}t} = k_p^I[S] - k_d^I[I] - k_r^T[T][I], \tag{2.10}$$

$$\frac{\mathrm{d}[T]}{\mathrm{d}t} = k_p^T[P_T] - k_d^T[T] - k_r^T[I][T], \tag{2.11}$$

$$\frac{\mathrm{d}[A]}{\mathrm{d}t} = k_p^A[P_A] - k_d^A[A] - k_r^A[I][A] \tag{2.12}$$

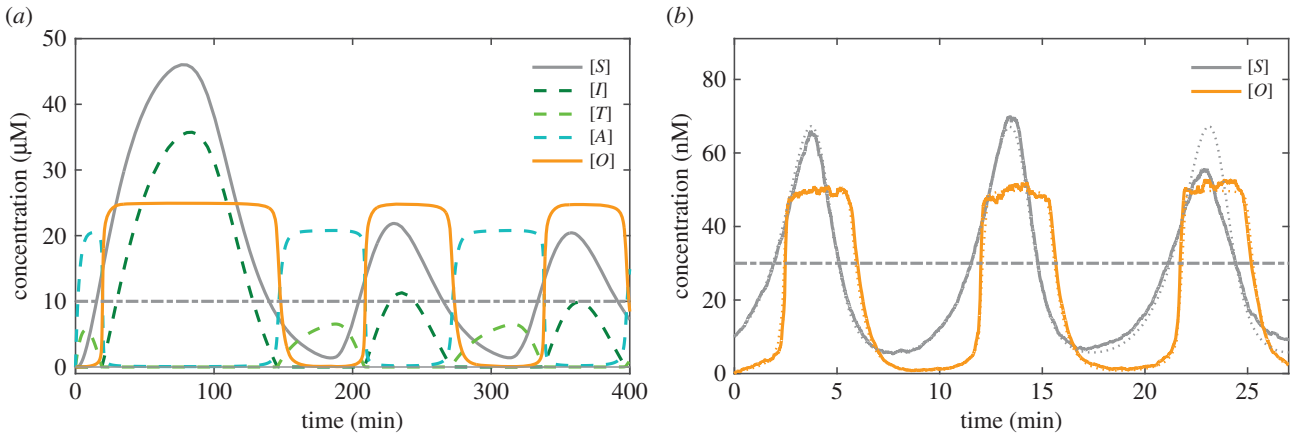

Figure 1. Timing response of the biomolecular comparator for different oscillatory source species. (*a*) Simulated timing response (mass action using equations (2.10)–(2.13)) of the comparator to a synthetic transcriptional oscillator [6]. The threshold and the high output concentration of the comparator are set to be 10 and 25 μM, respectively. Here, $k_p^I = k_d^I = 0.0031\ \mathrm{s}^{-1}$, $[P_T] = [P_A] = 20\ \mu\mathrm{M}$, $k_p^T = 0.0015\ \mathrm{s}^{-1}$, $k_d^T = 0.004\ \mathrm{s}^{-1}$, $k_p^A = 0.0067\ \mathrm{s}^{-1}$, $k_d^A = 0.0064\ \mathrm{s}^{-1}$, $k_d^O = 0.0054\ \mathrm{s}^{-1}$, $k_r^A = 0.06\ \mu\mathrm{M}^{-1}\ \mathrm{s}^{-1}$ and $k_r^T = 2.9\ \mu\mathrm{M}^{-1}\ \mathrm{s}^{-1}$. *T* and *A* are out of phase with respect to the source species because their first derivatives are proportional to $-[I]$ as shown in equations (2.11) and (2.12). The dash-dot line corresponds to the threshold above which the oscillator is determined by the comparator to be on. (b) Time trajectory of stochastic kinetics of a comparator circuit applied to a Lotka–Volterra oscillator [21] (electronic supplementary material, section S2). Here, the threshold of the comparator (dashed line) is 30 nM (903 molecules) and the high output of the comparator was designed to be 50 nM (1505 molecules). $[P_T] = [P_A] = 20$ nM, $k_p^I = k_d^I = k_d^T = k_d^A = k_d^O = 0.03\ \mathrm{s}^{-1}$, $k_p^T = 0.044\ \mathrm{s}^{-1}$, $k_p^A = 0.073\ \mathrm{s}^{-1}$, $k_r^A = 0.15\ \mathrm{nM}^{-1}\ \mathrm{s}^{-1}$ and $k_r^T = 2.92\ \mathrm{nM}^{-1}\ \mathrm{s}^{-1}$. The dotted and solid lines are, respectively, the results of deterministic mass action (normalized to the reaction volume) and stochastic kinetic simulations. (Online version in colour.)

and
$$\frac{\mathrm{d}[O]}{\mathrm{d}t} = k_r^A[I][A] - k_d^O[O]. \tag{2.13}$$

Equations (2.10)–(2.13) allow us to determine what output *O* is produced by a given dynamic input *S*.

In this paper, we will explore the use of this comparator when several time-scale separations are incorporated between different subsets of comparator reactions. We will first define these time-scale separations qualitatively, then determine quantitatively how much separation is required to achieve particular performance metrics. In this regime, we will also show how to tune the comparator's amplitude and timing responses by tuning specific rate parameters. Finally, we will consider what happens when these constraints are violated.

The times taken for $[I]$ to rise or fall to its high or low steady states are determined by the rate at which *I* is degraded, so k_d^I should be fast enough to follow the gradient changes of the source species in the absence of *T* and *A* (equations (2.10)–(2.12)). Similarly, k_d^O determines the concentration changes in *O* (equation (2.13)). Therefore, in order to ensure that *O* quickly changes between its low and high state and between its high and low state, k_d^I and k_d^O should be faster than the rate at which *S* is produced and degraded respectively. These requirements can be stated as $\{k_d^I, k_d^O\} \gg \max\{1/T_{\mathrm{sr}}, 1/T_{\mathrm{sf}}\}$, where T_{sr} and T_{sf} are the time taken by the source species to reach its highest concentration from its lowest and vice versa.

While the input species is produced, intermediates must perform thresholding and amplifying operations at a much faster rate than the degradation rates for the output species to reach its high and low values. The thresholding species *T* should degrade the predefined threshold concentration of *I* very rapidly compared with other reactions involving *I*, so that the minimum value of *O* will be close to zero when *I* is zero. This requires $k_r^T[I]_{\max} \gg k_r^A[I]_{\max} \gg \max\{k_d^I, k_d^T\}$. Moreover, the design constraint $k_r^A[I]_{\max} \gg k_d^A$ ensures that *A* degrades rapidly as soon as *I* increases from its minimum value (equation (2.12)). Together, these requirements can be expressed as $k_r^T[I]_{\max} \gg k_r^A[I]_{\max} \gg \max\{k_d^I, k_d^T, k_d^A\}$ and $\{k_d^I, k_d^O\} \gg \max\{1/T_{\mathrm{sr}}, 1/T_{\mathrm{sf}}\}$.

3. Results

3.1. Model validation

To verify that the comparator is able to produce a robust on and off signal in response to a typical input of a biomolecular oscillator, we designed a model composite system consisting of a transcriptional oscillator recently constructed by Franco *et al.* [6] using estimated rate constants for that system and the comparator. The oscillator contains a transcriptional activation pathway and a transcriptional repression pathway connected in a feedback loop through synthetic genes and produces an oscillatory response in a certain range of parameters [6] (electronic supplementary material, section S1). Using rate constants that are feasible in either *in vivo* or *in vitro* systems, the comparator is able to produce a consistent high signal level given the input from the biomolecular oscillator, so long as the amplitude of the source species is above the threshold (figure 1*a*).

We also expect that the oscillator should be able to produce a robust output signal even when the input signal contains random fluctuations in its concentration, provided that these fluctuations do not cross the on/off concentration threshold [22]. To test this hypothesis, we conducted stochastic kinetic simulations using the Gillespie algorithm [23]. For this simulation, we considered a Lotka–Volterra oscillator's output as an input signal to the comparator (electronic supplementary material, section S2). The comparator's response in the stochastic kinetic simulations lacked the variations in amplitude seen in the input signal (figure 1*b*). This simulation suggests that the comparator's output can be independent of both variations in the amplitude limits and fluctuations in the source species concentration. The closeness between the stochastic (solid line) and deterministic (dotted line) solution for *O* and also for *I*, *T*, *A* (electronic supplementary material, figure S4*a*) demonstrates the robustness of the comparator design when we adhere to the constraints imposed by the time-scale separations described above.

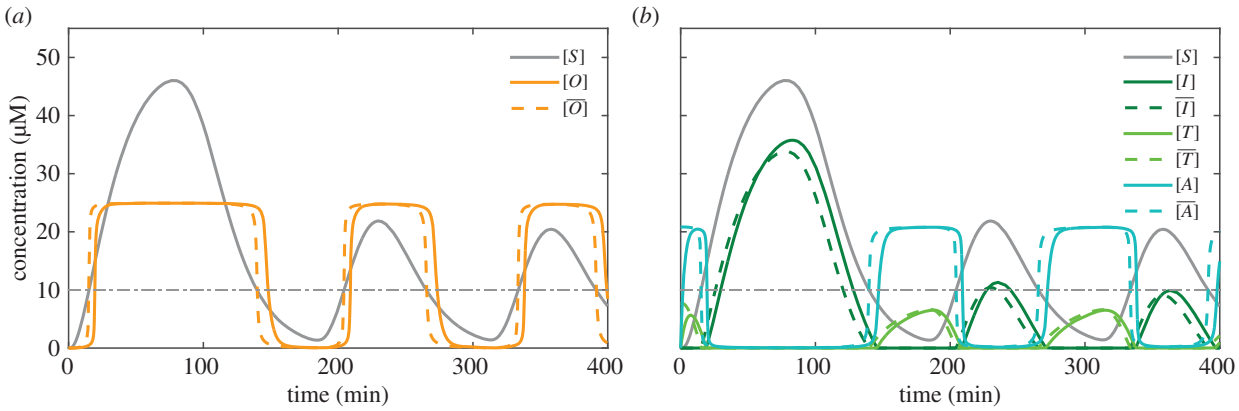

Figure 2. For typical inputs, the response of the comparator approaches its steady-state response. (*a*) The response of *O* (determined by numerical integration) to the input signal in figure 1*a* compared with the steady-state output signal $\overline{[O]}$. (*b*) *I*, *T* and *A* for the system in (*a*) compared with $\overline{[I]}$, $\overline{[T]}$ and $\overline{[A]}$. The intermediate species also remain close to their steady-state values. Here, $k_p^I = k_d^I = 0.0031\ \text{s}^{-1}$, $[P_T] = [P_A] = 20\ \mu\text{M}$, $k_p^T = 0.0015\ \text{s}^{-1}$, $k_d^T = 0.004\ \text{s}^{-1}$, $k_p^A = 0.0067\ \text{s}^{-1}$, $k_d^A = 0.0064\ \text{s}^{-1}$, $k_d^O = 0.0054\ \text{s}^{-1}$, $k_r^A = 0.06\ \mu\text{M}^{-1}\ \text{s}^{-1}$ and $k_r^T = 2.9\ \mu\text{M}^{-1}\ \text{s}^{-1}$. (Online version in colour.)

3.2. Comparator species concentrations stay close to their steady-state values

In the limit of a difference in time scales, the comparator should reach equilibrium before the output from the oscillator is able to change. Thus, we can estimate the performance of the module by calculating the steady-state behaviour of the module system. Some algebra shows that the steady state is given by

$$\left.\begin{aligned} \overline{[I]} &= \frac{k_p^I[S]}{k_d^I + k_r^T\overline{[T]}},\quad \overline{[T]} = \frac{k_p^T[P_T]}{k_d^T + k_r^T\overline{[I]}} \\ \text{and}\qquad \overline{[A]} &= \frac{k_p^A[P_A]}{k_d^A + k_r^A\overline{[I]}},\quad \overline{[O]} = \frac{k_r^A}{k_d^O}\overline{[I]}\,\overline{[A]}, \end{aligned}\right\} \tag{3.1}$$

where bars denote the steady-state response to a constant input *S*. We compared the response of the comparator in the system in figure 1*a* with the steady-state response for [*S*] at each time (figure 2*a*), and found that the two solutions produce similar outputs. *I*, *T* and *A* concentrations produced during the comparator's operation also remain close to their steady-state values (figure 2*b*). Moreover, using contraction theory [24,25], we found that the output of the comparator always produces a periodic response for the cases when the source species vary periodically (electronic supplementary material, section S3).

We can also evaluate the stability of the steady-state response of the comparator to local perturbations through local stability analysis. We start by linearizing the coupled first-order nonlinear differential equations at the steady state ($\overline{[I]}$, $\overline{[T]}$, $\overline{[A]}$, $\overline{[O]}$), which is determined by equating equations (2.10)–(2.13) to zero. After calculating the Jacobian matrix, we calculated the eigenvalues of the system and determined its local behaviour around the equilibrium point (electronic supplementary material, section S4). Specifically,

$$\left.\begin{aligned} \lambda_{1,2} &= -k_d^I - k_r^T\overline{[T]} - k_d^T - k_r^T\overline{[I]} \\ &\quad \pm \sqrt{\left(-k_d^I - k_r^T\overline{[T]} + k_d^T + k_r^T\overline{[I]}\right)^2 - 4(k_r^T)^2\overline{[I]}\,\overline{[T]}} \\ \text{and}\qquad \lambda_3 &= -k_d^A - k_r^A\overline{[I]},\ \ \lambda_4 = -k_d^O. \end{aligned}\right\} \tag{3.2}$$

Even though $\lambda_{1,2}$ are complex for some parameter values, all the eigenvalues of the Jacobian have negative real parts for arbitrary choices of the parameters (electronic supplementary material, section S4), demonstrating that small deviations in the concentrations of the input, intermediates and output species decay with time. Moreover, the rate at which the perturbed response approaches the steady state is governed by the largest eigenvalue (closest to the origin). It can be inferred from equation (3.2) that $\lambda_{1,2}$ and λ_3 will be closest to the origin when $\overline{[I]}$ and $\overline{[T]}$ are minimum. For a typical oscillator input, the minimum steady-state values of $\overline{[I]}$ and $\overline{[T]}$ will be close to zero, and so by increasing the degradation rates (k_d^I, k_d^T, k_d^A and k_d^O), the response times of *I*, *T*, *A* and *O* can be improved.

To illustrate this, we varied the degradation rates and the production rates in tandem for the comparator and found that, with larger degradation rates, the comparator responds more quickly (figure 3*a*). In this simulation, for simplicity, we considered k_d^I, k_d^T, k_d^A and k_d^O to be the same. However, for practical purposes, these rates can be different as long as the discussed time-scale separations between oscillator and comparator rates are maintained.

3.3. The comparator output spends most of its time at its maximum or minimum value

We now demonstrate analytically that when $k_r^T[I]_{\max} \gg k_r^A[I]_{\max} \gg \max\{k_d^I, k_d^T, k_d^A\}$ and $\{k_d^I, k_d^O\} \gg \max\{1/T_{\text{sr}}, 1/T_{\text{sf}}\}$, the comparator converts an oscillatory *S* species into an output species *O* that switches rapidly between predefined high and low states with a negligible transition time. First, we find the conditions where *O* reaches its maximum and minimum values and what these maximum and minimum values are as a function of the parameters of the system. We then determine what fraction of the time the comparator's output satisfies these conditions, and, therefore, the fraction of time the output spends in the on and off states as opposed to in the intermediate states. Where possible, we also describe the degree of separation between each of these variables required to achieve the desired performance. Assuming that the comparator operates much faster than [*S*] evolves, the dynamic responses of *I*, *T*, *A* and *O* can be effectively approximated by their steady-state responses (equation (3.1)). We can express $\overline{[O]} \approx [O]$ in terms of [*S*] and $\overline{[T]}$ using equation (3.1),

$$\overline{[O]} = \frac{k_p^A[P_A]}{k_d^O}\frac{[S]}{[S] + k_r^T/k_r^A(k_d^A/k_p^I)\overline{[T]} + (k_d^A/k_r^A)\ (k_d^I/k_p^I)}, \tag{3.3}$$

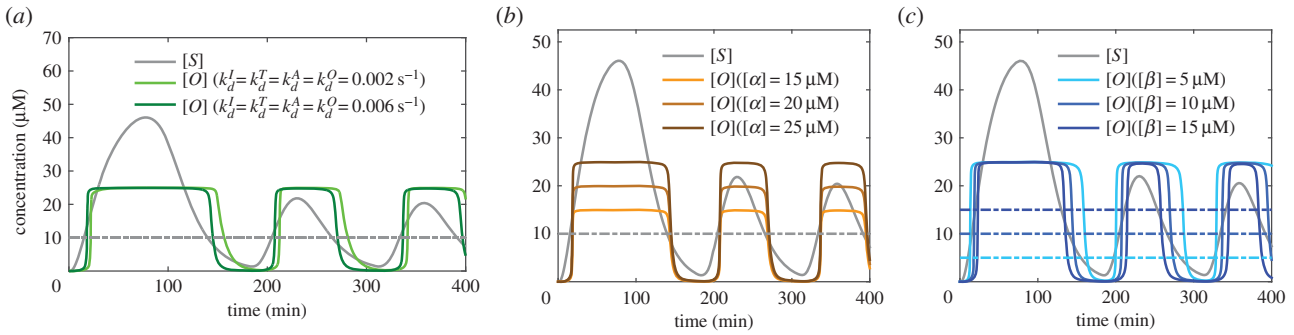

Figure 3. Varying specific parameters of the comparator can control the response time, amplitude and duty cycle of the comparator's output. Parameter dependencies of the biomolecular comparator for $[P_A] = 25\ \mu M$, $[P_T] = 10\ \mu M$, $k_d^I = k_d^T = k_d^A = k_d^O = 0.006\ s^{-1}$, $k_p^I = k_d^I$, $k_p^T = k_d^T$, $k_p^A = k_d^A$, $k_r^A = 0.06\ \mu M^{-1}\ s^{-1}$ and $k_r^T = 3\ \mu M^{-1}\ s^{-1}$ unless otherwise specified. Here, S is the output of the *in vitro* transcriptional oscillator while $[O]$ is calculated by numerically integrating equations (2.10)–(2.13). (*a*) Increasing the degradation rates while keeping $k_r^A = 10^7 \times k_d^A$ and $k_r^T = 45 \times k_r^A$ improves the response time. (*b*) Changing $[\alpha]$ (the amplitude of the comparator) changes the maximum concentration of O, while (*c*) changing $[\beta]$ (the threshold limit) changes the on/off threshold of the comparator, modifying its duty cycle (percentage of on signal over the period). (Online version in colour.)

where $\overline{[T]}$ can be expressed in terms of $[S]$ using equation (3.2),

$$\overline{[T]} = \left(-\frac{k_d^I}{2k_r^T} - \frac{k_p^I}{2k_d^T}[S] + \frac{k_p^T[P_T]}{2k_d^T}\right) \pm \sqrt{\left(\frac{k_d^I}{2k_r^T} + \frac{k_p^I}{2k_d^T}[S] - \frac{k_p^T[P_T]}{2k_d^T}\right)^2 - \frac{k_p^T[P_T]}{k_d^T}\frac{k_d^I}{k_r^T}}. \quad (3.4)$$

It can be inferred from equation (3.3) that the transfer characteristic of the comparator is a Hill-function-like response (electronic supplementary material, section S5).

3.4. The comparator's maximum output concentration

From equation (3.3), it is clear that $\overline{[O]}$ monotonically increases with $[S]$ and, that $\overline{[O]}$ monotonically decreases with $\overline{[T]}$. Therefore, $\overline{[O]}$ reaches its maximum value when $[S]$ is at its maximum and $\overline{[T]}$ is at its minimum. Thus, we can conclude that $\overline{[T]}$ is out of phase with $\overline{[O]}$, whereas $[S]$ is in phase with $\overline{[O]}$. We can therefore use equation (3.3) to express $\overline{[O]}_{max}$ as a function of the maximum value of $[S]$ and the minimum value of $\overline{[T]}$,

$$\overline{[O]}_{max} = \frac{k_p^A[P_A]}{k_d^O}\frac{[S]_{max}}{[S]_{max} + (k_r^T/k_r^A)(k_d^A/k_p^I)\overline{[T]}_{min} + (k_d^A/k_r^A)(k_d^I/k_p^I)}. \quad (3.5)$$

Thus, when

$$[S]_{max} \gg \frac{k_r^T}{k_r^A}\frac{k_d^A}{k_p^I}\overline{[T]}_{min} + \frac{k_d^A}{k_r^A}\frac{k_d^I}{k_p^I}, \quad (3.6)$$

we have that $\overline{[O]}_{max} \approx k_p^A[P_A]/k_d^O$. This is the high level of the output of the comparator and, for simplicity, we define it as $[\alpha]$. Equation (3.6) holds for the comparators we designed here. The production of I is catalysed by S (reaction (2.1)), so I follows S and therefore is also in phase with O. Because T is out of phase with O, it must also be out of phase with I. Thus, when $\overline{[T]} = \overline{[T]}_{min}$, $\overline{[I]}$ must be $\overline{[I]}_{max}$. Because by assumption

$$\frac{k_r^T}{k_d^T}\overline{[I]}_{max} \gg 1, \quad (3.7)$$

we can rewrite the steady-state expression of $\overline{[T]}$ (in equation (3.1)) as

$$\overline{[T]}_{min} = \frac{k_p^T[P_T]}{k_r^T\overline{[I]}_{max}}. \quad (3.8)$$

By replacing $\overline{[T]}_{min}$ in the steady-state expression of $\overline{[I]}$ (equation (3.1)), we see that $\overline{[I]}_{max} = [S]_{max} - [\beta]$, where $[\beta] = k_p^T[P_T]/k_d^I$. Now by replacing $\overline{[T]}_{min}$ (equation (3.8)) in equation (3.6) and using the fact that $\overline{[I]}_{max} = [S]_{max} - [\beta]$, equation (3.6) can be simplified to

$$\frac{k_r^A}{k_d^A}([S]_{max} - [\beta]) \gg 1. \quad (3.9)$$

Therefore, when $k_r^T\overline{[I]}_{max} \gg k_d^T$ and $k_r^A\overline{[I]}_{max} \gg k_d^A$, the output species will reach its maximum value.

3.5. The comparator's minimum output concentration

In a case where equations (3.7) and (3.9) are satisfied, numerical simulations show that the amplitude of the comparator's high output will be α (figure 3*b*) and the threshold point will be β (figure 3*c*). It should be noted that here $\overline{[I]}_{max}$ is $[S]_{max} - [\beta]$. Now, to find the minimum concentration of O and the conditions when $[O]$ reaches this minimum concentration $\overline{[O]}_{min}$, we rewrite equation (3.3) using the in-phase and out-of-phase behaviour of S and T with O, respectively:

$$\overline{[O]}_{min} = [\alpha]\frac{[S]_{min}}{[S]_{min} + (k_r^T/k_r^A)(k_d^A/k_p^I)\overline{[T]}_{max} + (k_d^A/k_r^A)(k_d^I/k_p^I)}. \quad (3.10)$$

From the steady-state expression of $\overline{[T]}$ (equation (3.1)), we infer that $\overline{[T]}_{max}$ is $k_p^T[P_T]/k_d^T$, which occurs when $[I]$ is close to zero as T and I are out of phase. Using this, we rewrite equation (3.10) as

$$\overline{[O]}_{min} = [\alpha]\frac{[S]_{min}}{[S]_{min} + (k_d^A/k_r^A)(k_d^I/k_p^I)((k_r^T/k_d^T)[\beta] + 1)}. \quad (3.11)$$

Thus, when

$$\frac{k_d^A}{k_r^A}\frac{k_d^I}{k_p^I}\left(\frac{k_r^T}{k_d^T}[\beta] + 1\right) \gg [S]_{min}, \quad (3.12)$$

$$\overline{[O]}_{min} = \frac{k_p^I}{k_d^I}\frac{k_r^A}{k_d^A}\frac{[\alpha][S]_{min}}{((k_r^T/k_d^T)[\beta] + 1)}. \quad (3.13)$$

Equations (3.12) and (3.13) are long, but some intuitive notion of their meaning can be gained from the simple case where $k_p^I = k_d^I = k_d^T = k_d^A = k_d^O$ and $\overline{[I]}_{max}$ and $[\beta]$ are of the same order. In this case, using equation (3.7) we can simplify

equations (3.12) and (3.13) to

$$\frac{k_r^T}{k_r^A}[\beta] \gg [S]_{\min} \tag{3.14}$$

and

$$\overline{[O]}_{\min} = \frac{[\alpha]}{[\beta]}\frac{k_r^A}{k_r^T}[S]_{\min}. \tag{3.15}$$

3.6. The transition time of *O*

Now we derive conditions where *O* spends most of its time in low or high states and negligible time in the intermediate states. Assuming equations (3.7), (3.9) and (3.12) are true, *O* will be high whenever $[S] > [\beta]$ and low otherwise when the time it takes for *I* to change from $[I]_{\min} \rightarrow [I]_{\max}$ and the time it takes for *I* to change from $[I]_{\max} \rightarrow [I]_{\min}$ are smaller than T_{sr} ($[S]_{\min} \rightarrow [S]_{\max}$) and T_{sf} ($[S]_{\max} \rightarrow [S]_{\min}$) respectively. For simplicity, here we derive the requirements assuming that k_p^I is the same as k_d^I so that $[I]_{\min} = [S]_{\min}$ and $[I]_{\max} = [S]_{\max}$ in the absence of *T* and *A* (equations (2.10)–(2.12)). However, these requirements are not essential for the comparator to function and for *O* to spend most of its time in its high and low states. Under these conditions, when *T* approaches $[\overline{T}]_{\min}$ and [*I*] has not yet started increasing, equation (2.10) acts as a standard proportional controller. During the transition, *I* must go from its initial concentration to its maximum value $[S]_{\max} - [\beta]$, whereas *S* is changing from $[S]_{\min} \rightarrow [S]_{\max}$ with time constant T_{sr}. Similarly, *I* should degrade quickly from its maximum value ($[S]_{\max} - [\beta]$) to its minimum value while *S* is changing from $[S]_{\max} \rightarrow [S]_{\min}$ in time T_{sf}. These constraints are satisfied when (electronic supplementary material, section S6)

$$k_d^I \geq \max\left\{\frac{1}{T_{sr}}\ln\left(\frac{([S]_{\max}-[\beta])}{([S]_{\max}-[\beta])-\overline{[I]}_{\max}}\right), \frac{1}{T_{sf}}\ln\left(\frac{([S]_{\max}-[\beta])}{\overline{[I]}_{\min}}\right)\right\}. \tag{3.16}$$

It should be noted that k_p^I need not be exactly the same as k_d^I. When k_p^I is different from k_d^I, the comparator's output might become high at a different threshold concentration from $[\beta]$, but the system still can produce a robust on and off response (electronic supplementary material, figure S6*a*).

While k_d^I determines the response time of *I*, k_d^O and the time-scale separation between k_r^A and k_d^A (equation (3.9)) determine the time *O* takes to transition between its low and high states. A similar relation between k_d^O and $\{T_{sr}, T_{sf}\}$ can be derived using equation (3.13). The results are (electronic supplementary material, section S6)

$$k_d^O \geq \max\left\{\frac{1}{T_{sr}}\ln\left(\frac{[\alpha]}{[\alpha]-\overline{[O]}_{\max}}\right), \frac{1}{T_{sf}}\ln\left(\frac{[\alpha]}{\overline{[O]}_{\min}}\right)\right\}. \tag{3.17}$$

Moreover, k_d^T should be fast enough so that *T* degrades quickly in the absence of *I* and reaches its minimum value before *I* is produced. However, the upper bound of k_d^T is determined by equations (3.7) and (3.12). Finally, $k_d^A \geq k_d^O$ in order to avoid an initial 'overshoot' of the comparator's output, which happens when *O* changes from $[O]_{\min}$ to $[O]_{\max}$ and k_d^A is slower than k_d^O (electronic supplementary material, figure S6*b*).

An understanding of how the design of the comparator affects its operation in combination with a given biomolecular oscillator is important, because different biomolecular oscillators produce different temporal responses [3,6,7]; we can therefore use this understanding to design a comparator that can work with a particular biomolecular oscillator. Moreover, by properly altering the parameters, we can also design the comparator's timing response. To test our analysis of the design requirements for the degradation rates (k_d^I, k_d^T, k_d^A and k_d^O), and k_r^A and k_r^T, we conducted systematic numerical simulations while varying these parameters (electronic supplementary material, section S7). Initially, during this analysis, we assumed that all the degradation rates were the same. These rates were varied from 0.0006 to 0.06 s^{-1}; switching between high and low output values occurred quickly for 0.006 and 0.06 s^{-1}. This fast switching is in agreement with equations (3.16) and (3.17), because in order to maintain the time-scale separation between $\{k_d^I, k_d^O\}$ and $\max(1/T_{sr}, 1/T_{sf})$, k_d^I and k_d^O need to be much higher than 0.0002 s^{-1}. Similarly, we varied k_r^A/k_d^A and k_r^T/k_r^A and found that these ratios determine whether *O* will reach its maximum and minimum values or not, as suggested by our analysis.

In any practical system, however, the degradation rates of *I*, *T*, *A* and *O* will not all be exactly the same. Therefore, to quantify the effects of differences in these degradation rates, we varied each degradation rate randomly within a bound of 20% variations from a mean value (0.006 s^{-1}) while keeping β, α, P_T, P_A, k_p^T, k_p^A, k_r^A and k_r^T fixed and considering $k_d^A \geq k_d^O$. In each simulation with randomized parameter values, we found that the qualitative response remains the same (electronic supplementary material, figure S10), with slight variations in the fraction of time spent in the on versus off states. Similar variations in [*O*] were observed when we varied both these rates and k_r^T and k_r^A while keeping β, α, P_T, P_A, k_p^T and k_p^A fixed (electronic supplementary material, figure S11).

Further insights about the relationship between the degradation rates and the range of periods of the source species for which a valid output can be produced can be gained by frequency analysis. We found that the output amplitude of the comparator in figure 1*a* remains close to $[\alpha] = 25$ µM in a wide range of low oscillator input frequencies (electronic supplementary material, section S9).

3.7. Oscillator-specific comparator design

The tunability of the dynamic and steady-state properties of the comparator make it possible to optimize the comparator reactions to process the outputs of a variety of molecular oscillators. To explore this possibility, we designed two biomolecular comparators for two different biomolecular oscillators: the p53-Mdm2 negative feedback composite network motif, which consists of both protein–protein interaction and transcriptional processes [3,26] and an *in vitro* predator–prey oscillator based on synthetic components [7]. The p53-Mdm2 oscillator is a well-studied *in vivo* oscillator [3]. The predator–prey oscillator produces a periodic output based on opposing DNA polymerization–depolymerization reactions [7].

In order to correctly process the output of the p53-Mdm2 and predator–prey oscillators using the biomolecular comparator, system parameters such as reaction rate constants α and β needed to be tuned as these oscillators differ in their timing and amplitude response compared with the previously discussed transcriptional oscillator. We used equations (3.9), (3.12), (3.16) and (3.17) to choose values of production and degradation rates and k_r^A, k_r^T, β, α, P_T and

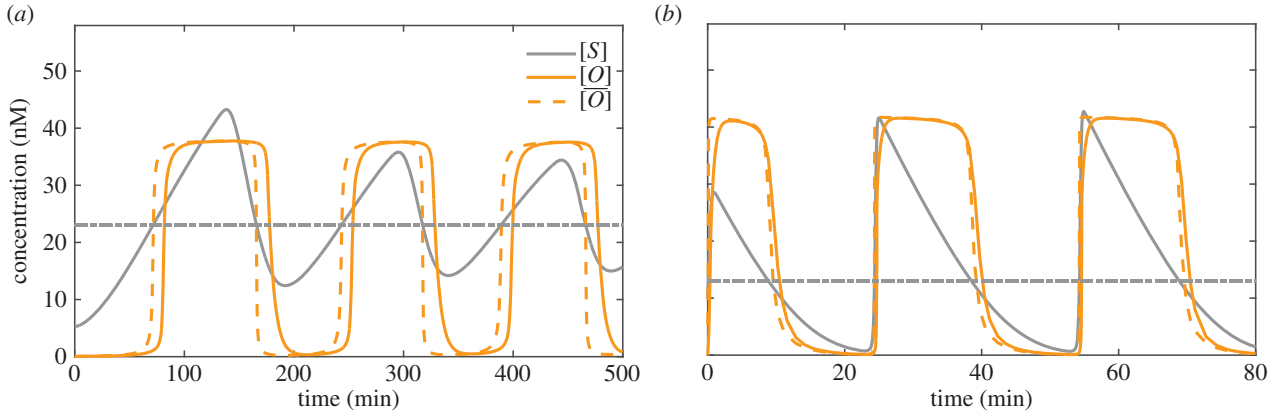

Figure 4. The output of different biomolecular oscillators with different oscillatory dynamics can be transformed into digital output signals using comparators. (*a*) The p53-Mdm2 composite network motif consisting of proteins that are transcribed and then interact produces damped oscillations in the presence of an external excitation signal (stress) [3]. Shown here is a simulated output signal from this oscillator along with the output of a comparator that processes the signal. Parameter values were selected as described in the text: $[\alpha] = 38$ nM, $[\beta] = 23$ nM, $k_p^I = k_d^I = 0.0017\ \mathrm{s}^{-1}$, $[P_T] = [P_A] = 30$ nM, $k_p^T = 0.0013\ \mathrm{s}^{-1}$, $k_d^T = 0.002\ \mathrm{s}^{-1}$, $k_p^A = 0.004\ \mathrm{s}^{-1}$, $k_d^A = 0.0037\ \mathrm{s}^{-1}$, $k_d^0 = 0.0031\ \mathrm{s}^{-1}$, $k_r^A = 0.03\ \mathrm{nM}^{-1}\ \mathrm{s}^{-1}$ and $k_r^T = 2.9\ \mathrm{nM}^{-1}\ \mathrm{s}^{-1}$. (*b*) The output of an *in vitro* predator–prey-based oscillator and the comparator's output signal [7]. Here, $[\alpha] = 42$ nM, $[\beta] = 13$ nM, $k_p^I = k_d^I = 0.05\ \mathrm{s}^{-1}$, $[P_T] = [P_A] = 30$ nM, $k_p^T = 0.022\ \mathrm{s}^{-1}$, $k_d^T = 0.03\ \mathrm{s}^{-1}$, $k_p^A = 0.043\ \mathrm{s}^{-1}$, $k_d^A = 0.04\ \mathrm{s}^{-1}$, $k_d^0 = 0.026\ \mathrm{s}^{-1}$, $k_r^A = 0.2\ \mathrm{nM}^{-1}\ \mathrm{s}^{-1}$ and $k_r^T = 3\ \mathrm{nM}^{-1}\ \mathrm{s}^{-1}$. In (*a*,*b*), the comparator's dynamic output (solid) remains close to its steady-state value for the given input signal (dashes). (Online version in colour.)

P_A so that both comparators operate stably and have rates that could allow them to be implemented in experiments.

For example, for the p53-Mdm2 oscillator, T_{sr} and T_{sf} are around 90 and 50 min, respectively [26]. Using equation (3.17), we calculated that O's minimum value will be 0.01% of its high steady-state value $[\alpha]$ for $k_d^O = 0.0031\mathrm{s}^{-1}$. To allow O to spend almost equal time in its high and low states, we set $\beta = 23$ nM. We then used equation (3.16) to set k_d^I and k_p^I to be $0.0017\ \mathrm{s}^{-1}$, so that I's maximum concentration will be 99.99% of its high steady-state value. We chose k_d^T to be $0.002\ \mathrm{s}^{-1}$, so that T reaches its minimum value before I is produced. $[P_T]$, $[P_A]$, k_p^T and k_p^A can be selected arbitrarily as long as $k_p^T[P_T] \approx k_d^I[\beta]$ and $k_p^A[P_A] \approx k_d^O[\alpha]$. These conditions ensure that the threshold concentration is $[\beta]$ and the maximum concentration of O is $[\alpha]$ respectively. Finally, assuming $k_d^A = 1.5 \times k_d^O$, we chose k_r^A and k_r^T to satisfy equations (3.9) and (3.12). A similar calculation was done for the predator–prey oscillator.

Using the mathematical models of p53-Mdm2 and predator–prey oscillators proposed in [26] and [7], respectively, numerical simulations of the resulting composite oscillator–comparator systems indicated that the oscillatory output responses of p53 protein and predator species both are translated into the desired on and off signals by the comparators we designed (figure 4). While it is not possible to accurately choose reaction rates in experimental systems, an understanding of how different relative reaction rates influence different aspects of the comparator's behaviour will make it possible to efficiently design and tune an experimental implementation.

4. Discussion

We have described a biomolecular comparator which can, given an oscillatory molecular species as input, produce an output with a periodic square wave signal output that follows the period of the input oscillator. By following well-defined rules about how to set the reaction rates, we show how to tune the threshold that determines when the output signal should be on or off, the concentrations of the comparator's output in its on and off states and the time to transition between these two states. To validate the biomolecular comparator's operation, we used different rate constants that can be realized practically *in vitro* using either DNA strand displacement reactions [11] or transcriptional circuits [27] or *in vivo* with RNA circuits or proteins [12–14,28,29]. For example, one potential implementation of the comparator would be within a system for RNA processing. S could function as an activator for RNA species I, which is otherwise unregulated. Another RNA T could silence I, perhaps by binding to it, and A could be either a protein or regulatory RNA that can release O in the presence of I. The difference in time scales between transcription and RNA binding and cofactor-assisted activation would make it possible to implement a system with the required separations of time scales. A growing set of tools for engineering *in vivo* RNA-based logic could be used to design these mechanisms [30–33]. *In vitro*, transcriptional circuits [13,34,35] or strand displacement circuits [9,36] could potentially also implement the mechanisms we describe.

This comparator could be used to rectify biomolecular oscillator signals with a wide variety of periods. It could also, in principle, be used to rectify other time-varying input signals, so long as the rates for the corresponding comparator satisfy the time-scale separations we have described. More generally, this work also suggests that modular biomolecular components could, in principle, quantitatively tune the behaviour of dynamical biomolecular systems. Such a practice could allow a variety of dynamical biomolecular signal processing elements to be rapidly implemented and scaled.

The well-defined timing characteristics of most potential biomolecular oscillator inputs mean that the comparator's output will be a robust clock signal, because the comparator filters fluctuations and noise in the oscillator amplitude. Cellular oscillators such as the cell cycle and circadian clock oscillators control a variety of downstream binary operations [4,5]. However, it is interesting to note that the timing behaviour of these oscillators is more essential for robust operations

than the amplitude response [2,3]. One possible explanation for this phenomenon is that oscillatory signals may be processed by downstream mechanisms analogous to the comparator whose outputs are not sensitive to amplitude variability. While no such processing mechanisms have been found to the authors' knowledge, well-characterized gene circuits and signal transduction pathways do incorporate the concept of ultrasensitivity applied here in order to control cellular behaviour reliably [37,38]. One well-studied example is the Notch–Delta signalling pathway, whose robust on/off response plays a critical role in pattern formation during cellular development [39].

Further work in this area might be motivated by the consideration of a variety of alternative designs for a comparator; for example, a discrete time signal-processing methodology might also be used to perform the desired operations on a time-varying species [40,41]. Finally, this work suggests a variety of other questions about how oscillatory signals might be processed by downstream coupled reaction modules. One problem of particular interest would be to control the output period, either by filtering fluctuations in an oscillator's period or by altering it such as by doubling or halving the period of the upstream oscillator.

Authors' contributions. D.K.A., E.F. and R.S. designed the research; D.K.A. and E.F. performed the research; D.K.A., E.F. and R.S. analysed the data; and D.K.A., E.F. and R.S. wrote the paper.

Competing interests. We declare we have no competing interests.

Funding. This work was supported in part by DOE grant SC0010595 to R.S. and E.F. (for modelling and the analysis herein), by NSF grant no. CMMI-1266402 to E.F. and NSF grant no. CCF-1161941 to R.S.

Acknowledgements. The authors thank Dominic Scalise for helpful discussions.

References

1. Goldbeter A. 1996 *Biochemical oscillations and cellular rhythms. The molecular bases of periodic and chaotic behaviour*. Cambridge, UK: Cambridge University Press.
2. Mihalcescu I, Hsing W, Leibler S. 2004 Resilient circadian oscillator revealed in individual cyanobacteria. *Nature* **430**, 81–85. (doi:10.1038/nature02533)
3. Lahav G, Rosenfeld N, Sigal A, Geva-Zatorsky N, Levine AJ, Elowitz MB, Alon U. 2004 Dynamics of the p53-Mdm2 feedback loop in individual cells. *Nat. Genet*. **36**, 147–150. (doi:10.1038/ng1293)
4. Tyson JJ, Csikasz-Nagy A, Novak B. 2002 The dynamics of cell cycle regulation. *Bioessays* **12**, 1095–1109. (doi:10.1002/bies.10191)
5. Barkai N, Leibler S. 2000 Biological rhythms: Circadian clocks limited by noise. *Nature* **403**, 267–268.
6. Franco E, Friedrichs E, Kim J, Jungmann R, Murray R, Winfree E, Simmel FC. 2011 Timing molecular motion and production with a synthetic transcriptional clock. *Proc. Natl Acad. Sci. USA* **108**, E784–E793. (doi:10.1073/pnas.1100060108)
7. Fujii T, Rondelez Y. 2013 Predator–prey molecular ecosystems. *ACS Nano*. **7**, 27–34. (doi:10.1021/nn3043572)
8. Robinson FNH. 1959 Nuclear resonance absorption circuit. *J. Sci. Instrum*. **36**, 481–487. (doi:10.1088/0950-7671/36/12/301)
9. Scalise D, Schulman R. 2014 Designing modular reaction-diffusion programs for complex pattern formation. *Technology* **2**, 55. (doi:10.1142/S2339547814500071)
10. Zhang DY, Winfree E. 2009 Control of DNA strand displacement kinetics using toehold exchange. *J. Am. Chem. Soc*. **131**, 17303–17314. (doi:10.1021/ja906987s)
11. Zhang DY, Seelig G. 2011 Dynamic DNA nanotechnology using strand-displacement reactions. *Nat. Chem*. **3**, 103–113. (doi:10.1038/nchem.957)
12. Mishra D, Rivera PM, Lin A, Del Vecchio D, Weiss R. 2014 A load driver device for engineering modularity in biological networks. *Nat. Biotechnol*. **32**, 1268–1275. (doi:10.1038/nbt.3044)
13. Franco E, Giordano G, Forsberg PO, Murray RM. 2014 Negative autoregulation matches production and demand in synthetic transcriptional networks. *ACS Synth. Biol*. **3**, 589–599. (doi:10.1021/sb400157z)
14. Hsiao V, de los Santos ELC, Whitaker WR, Dueber JE, Murray RM. 2015 Design and implementation of a biomolecular concentration tracker. *ACS Synth. Biol*. **4**, 150–161. (doi:10.1021/sb500024b)
15. Alon U. 2006 *An introduction to systems biology: design principles of biological circuits*. Boca Raton, FL: Chapman and Hall/CRC.
16. Strogatz SH. 1994 *Nonlinear dynamics and chaos: with applications to physics, biology, chemistry, and engineering*. Cambridge, MA: Perseus Books Group.
17. Del Vecchio D, Ninfa AJ, Sontag ED. 2008 Modular cell biology: retroactivity and insulation. *Mol. Syst. Biol*. **4**, 161. (doi:10.1038/msb4100204)
18. Buchler NE, Louis M. 2008 Molecular titration and ultrasensitivity in regulatory networks. *J. Mol. Biol*. **384**, 1106–1119. (doi:10.1016/j.jmb.2008.09.079)
19. Belle A, Tanay A, Bitincka L, Shamir R, O'Shea EK. 2006 Quantification of protein half-lives in the budding yeast proteome. *Proc. Natl Acad. Sci. USA* **103**, 13 004–13 009. (doi:10.1073/pnas.0605420103)
20. Soloveichik D, Seelig G, Winfree E. 2010 DNA as a universal substrate for chemical kinetics. *Proc. Natl Acad. Sci. USA* **107**, 5393–5398. (doi:10.1073/pnas.0909380107)
21. Freedman HI. 1998 *Deterministic mathematical models in population ecology*. New York, NY: Marcel Dekker.
22. Elf J, Paulsson J, Berg OG, Ehrenberg M. 2003 Near-critical phenomena in intracellular metabolite pools. *Biophys. J*. **84**, 154–170. (doi:10.1016/S0006-3495(03)74839-5)
23. Gillespie DT. 1977 Exact stochastic simulation of coupled chemical reactions. *J. Phys. Chem*. **81**, 2340–2361. (doi:10.1021/j100540a008)
24. Lohmiller W, Slotine JJE. 1998 On contraction analysis for non-linear systems. *Automatica* **34**, 683–696. (doi:10.1016/S0005-1098(98)00019-3)
25. Russo G, Di Bernardo M, Sontag ED. 2010 Global entrainment of transcriptional systems to periodic inputs. *PLoS Comput. Biol*. **6**, e1000739. (doi:10.1371/journal.pcbi.1000739)
26. Bar-Or RL, Maya R, Segel LA, Alon U, Levine AJ, Oren M. 2000 Generation of oscillations by the p53-Mdm2 feedback loop: a theoretical and experimental study. *Proc. Natl Acad. Sci. USA* **97**, 11 250–11 255. (doi:10.1073/pnas.210171597)
27. Kelly DP, Scarpulla RC. 2004 Transcriptional regulatory circuits controlling mitochondrial biogenesis and function. *Genes Dev*. **18**, 357–368. (doi:10.1101/gad.1177604)
28. Hendrix DA, Hong JW, Zeitlinger J, Rokhsar DS, Levine MS. 2008 Promoter elements associated with RNA Pol II stalling in the *Drosophila* embryo. *Proc. Natl Acad. Sci. USA* **105**, 7762–7767. (doi:10.1073/pnas.0802406105)
29. Mehta P, Goyal S, Wingreen NS. 2008 A quantitative comparison of sRNA-based and protein-based gene regulation. *Mol. Syst. Biol*. **4**, 221. (doi:10.1038/msb.2008.58)
30. Bloom RJ, Winkler SM, Smolke CD. 2014 A quantitative framework for the forward design of synthetic miRNA circuits. *Nat. Methods* **11**, 1147–1153. (doi:10.1038/nmeth.3100)
31. Green AA, Silver PA, Collins JJ, Yin P. 2014 Toehold switches: de-novo-designed regulators of gene expression. *Cell* **159**, 925–939. (doi:10.1016/j.cell.2014.10.002)
32. Strovas TJ, Rosenberg AB, Kuypers BE, Muscat RA, Seelig G. 2014 MicroRNA-based single-gene circuits buffer protein synthesis rates against perturbations. *ACS Synth. Biol*. **3**, 324–331. (doi:10.1021/sb4001867)
33. Chappell J, Takahashi MK, Lucks JB. 2015 Creating small transcriptional activating RNAs.

Nat. Chem. Biol. **11**, 214–220. (doi:10.1038/nchembio.1737)

34. Kim J, White KS, Winfree E. 2006 Construction of an *in vitro* bistable circuit from synthetic transcriptional switches. *Mol. Syst. Biol*. **1**, 68. (doi:10.1038/msb4100099)
35. Kim J, Winfree E. 2011 Synthetic *in vitro* transcriptional oscillators. *Mol. Syst. Biol*. **7**, 465. (doi:10.1038/msb.2010.119)
36. Chen X, Briggs N, McLain JR, Ellington AD. 2013 Stacking nonenzymatic circuits for high signal gain. *Proc. Natl Acad. Sci. USA* **110**, 5386–5391. (doi:10.1073/pnas.1222807110)
37. Ferrell Jr JE. 2002 Self-perpetuating states in signal transduction: positive feedback, double-negative feedback and bistability. *Curr. Opin. Cell Biol*. **14**, 140–148. (doi:10.1016/S0955-0674(02)00314-9)
38. Zhang Q, Bhattacharya S, Andersen ME. 2013 Ultrasensitive response motifs: basic amplifiers in molecular signalling networks. *Open Biol*. **3**, 130031. (doi:10.1098/rsob.130031)
39. Sprinzak D, Lakhanpal A, LeBon L, Santat LA, Fontes ME, Anderson GA, Garcia-Ojalvo J, Elowitz MB. 2010 *Cis*-interactions between Notch and Delta generate mutually exclusive signalling states. *Nature* **465**, 86–90. (doi:10.1038/nature08959)
40. Jiang H, Riedel MD, Parhi KK. 2012 Digital signal processing with molecular reactions. *IEEE Des. Test Mag*. **29**, 21–31. (doi:10.1109/MDT.2012.2192144)
41. Jiang H, Salehi SA, Riedel MD, Parhi KK. 2013 Discrete-time signal processing with DNA. *ACS Synth. Biol*. **2**, 245–254. (doi:10.1021/sb300087n)